The effects of magnetic nanoparticle properties on magnetic fluid hyperthermia

Ravi Kappiyoor, Monrudee Liangruksa, Ranjan Ganguly, and Ishwar K. Puri

Citation: Journal of Applied Physics **108**, 094702 (2010); doi: 10.1063/1.3500337
View online: http://dx.doi.org/10.1063/1.3500337
View Table of Contents: http://scitation.aip.org/content/aip/journal/jap/108/9?ver=pdfcov
Published by the AIP Publishing

The effects of magnetic nanoparticle properties on magnetic fluid hyperthermia

Ravi Kappiyoor,[1] Monrudee Liangruksa,[1] Ranjan Ganguly,[2] and Ishwar K. Puri[1,a)]
[1]*Department of Engineering Science and Mechanics, Virginia Polytechnic Institute, State University, Blacksburg, Virginia 24061, USA*
[2]*Department of Power Engineering, Jadavpur University, Kolkata 700098, India*

(Received 3 June 2010; accepted 8 September 2010; published online 10 November 2010)

Magnetic fluid hyperthermia (MFH) is a noninvasive treatment that destroys cancer cells by heating a ferrofluid-impregnated malignant tissue with an ac magnetic field while causing minimal damage to the surrounding healthy tissue. The strength of the magnetic field must be sufficient to induce hyperthermia but it is also limited by the human ability to safely withstand it. The ferrofluid material used for hyperthermia should be one that is readily produced and is nontoxic while providing sufficient heating. We examine six materials that have been considered as candidates for MFH use. Examining the heating produced by nanoparticles of these materials, barium-ferrite and cobalt-ferrite are unable to produce sufficient MFH heating, that from iron-cobalt occurs at a far too rapid rate to be safe, while fcc iron-platinum, magnetite, and maghemite are all capable of producing stable controlled heating. We simulate the heating of ferrofluid-loaded tumors containing nanoparticles of the latter three materials to determine their effects on tumor tissue. These materials are viable MFH candidates since they can produce significant heating at the tumor center yet maintain the surrounding healthy tissue interface at a relatively safe temperature. © *2010 American Institute of Physics*. [doi:10.1063/1.3500337]

I. INTRODUCTION

Cancer is a leading cause of human deaths.[1,2] Current treatments, such as surgery and chemotherapy, can have undesirable side effects, including harm to the surrounding healthy tissue. Hyperthermia is an alternative treatment that can destroy cancerous cells by significantly elevating the temperature of tumor cells while keeping that of the surrounding healthy tissue at a reasonable level.[3]

One method to induce hyperthermia is by use of ferrofluids, which are colloidal suspensions of magnetic nanoparticles (MNPs) in a nonpolar medium. These fluids can be magnetically targeted to cancerous tissue after intravenous application.[1] The magnetic particles extravasate into the tumor due to the high microvascular permeability and interstitial diffusion in neoplastic tissue.[4] Thereafter, the MNPs are heated by exposing the tumor to a high frequency alternating magnetic field, causing thermonecrosis of the embedding tissue. This process is called magnetic fluid hyperthermia (MFH).[3,5–9]

In order to examine the potential of hyperthermia as a viable alternative to chemotherapy and radioactive treatment, it is necessary to define what such a treatment would hope to accomplish. Temperatures in the range of 41–45 °C are enough to slow or halt the growth of cancerous tissue, but such heating can also damage healthy cells.[3] Thus, an ideal hyperthermia treatment should sufficiently increase the temperature of the tumor cells while maintaining the healthy tissue temperature below 41 °C. Ferrofluid-based thermotherapy can be also accomplished through thermoablation, which typically heats tissues up to 56 °C to cause their necrosis, coagulation, or carbonization by exposure to a noninvasive radio frequency ac magnetic field.[5] Local heat transfer from the nanoparticles increases the tissue temperature and ruptures the cell membranes.[10,11]

Iron oxide nanoparticles such as magnetite, or its oxidized form maghemite, are the most biocompatible agents for MFH.[9] These particles are typically coated with a biocompatible polymer to prevent their aggregation and biodegradation for *in vivo* applications. Platinum and nickel are also MNPs but are toxic and vulnerable to oxidation.[2]

MFH employing fine magnetic particles was first investigated by Gilchrist *et al.*[12] This work was followed by several *in vitro* and *in vivo* experiments to confirm the feasibility of magnetic particle use for MFH.[11,13–15] Numerical investigations have also allowed researchers to understand and improve MFH therapy in soft biological tissue by using models consisting of multiple homogeneous regions[16] that contain tumor and normal tissue.[15,17,18] These models have provided approaches for the proper particle dosage and distribution in the tumor, and the optimal particle properties and magnetic field strengths that minimize the side effects of MFH on healthy tissues.

For optimal MFH treatment, ferrofluid dosage should be minimal and yet provide sufficient heating. This depends upon factors such as the magnetic anisotropy constant of the nanoparticles, and the strength and frequency of the ac field. Previous investigations have considered specific ferrofluids to determine the optimal particle type and size[5,9,19] and the thermal response of tissue.[7] However, the literature does not provide guidance about the influence of both particle type and size on MFH under typical clinical conditions. There-

a)Electronic mail: ikpuri@vt.edu.

fore, we focus on the appropriate use of MNPs to heat soft tissue using an ac magnetic field[9] in this context.

When exposed to such an ac field, the MNPs dissipate magnetic energy into heat through both Brownian and Néel relaxations. Besides the strength and frequency of the alternating magnetic field,[20] the magnetic properties of an MNP also play an important role in heat generation and dissipation.[9,19] We account for the particle size distribution, saturation magnetization, and the material anisotropy constant. Since iron nanoparticles have both a large saturation magnetization[21] and a high Curie temperature (of 1043 K),[21] we consider iron and iron compound nanoparticles as primary choices for MFH.[9,19] Changing the nanoparticle size can significantly alter the ability of an MNP to generate heat,[9,22] making the determination of an optimum nanoparticle size necessary for a specified set of conditions.

Here, we present a thermodynamic analysis of ferrofluid magnetic heating and compare the performance of six different types of ferrofluids, namely those containing magnetite ($FeO \cdot Fe_2O_3$), maghemite (γ-Fe_2O_3), iron-platinum (FePt), iron-cobalt (FeCo), barium-ferrite ($BaFe_2O_4$), and cobalt-ferrite ($CoFe_2O_4$). We examine their performance for different magnetic field strengths, frequencies and particle radii. Thereafter, we investigate the heating of a tumor and the surrounding healthy tissue with suitable MFH ferrofluid candidates.

II. ANALYSIS OF MAGNETIC HEATING

A. Thermodynamic analysis

For a constant density system and an adiabatic process,[9]

$$dU = \delta Q + \delta W = \delta W = \vec{H} \,.\, d\vec{B}, \tag{1}$$

where dU denotes the internal energy change, δQ the heat input, δW the work done on the system, $\vec{H}$ the magnetic field intensity, and $\vec{B}$ the magnetic field. Upon integration,

$$\Delta U = -\mu_0 \oint M dH. \tag{2}$$

Here, μ_0 denotes the permeability of free space and M the magnetization of the material. Since an oscillating magnetic field is required to produce the Brownian and Néel relaxations during MFH, we assume that

$$H(t) = H_0 \cos(\omega t), \tag{3}$$

Using the Langevin equation[23] the magnetization of the nanoparticles

$$M_0(t) = M_{sat}\varphi\{\coth[L(t)] - 1/L(t)\}, \text{ where} \tag{4}$$

where M_{sat} denotes saturation magnetization of the material. The Langevin parameter $L(t)$ is defined as

$$L(t) = (4\pi R^3/3)\mu_0 M_{sat} H(t)/(kT), \tag{5}$$

where R is the nanoparticle radius, k the Boltzmann constant (1.38×10^{-23} J K^{-1}), and T the absolute temperature (Kelvin). The ferrofluid susceptibility

$$\chi_0 = M_0(t)/H(t), \quad \chi' = \chi_0/[1 + (\omega\tau)^2],$$

TABLE I. Physical properties of soft tissue (Ref. 19).

Tissue	ρ (kg/m^3)	λ (W/m/°C)	c (J/kg/°C)	w_b (s^{-1})
Tumor (w/o MNP)	1060	0.502	3600	6.4
Blood	1000	N/A	4180	6.4

$$\chi'' = (\omega\tau\chi_0)/[1 + (\omega\tau)^2], \tag{6}$$

where χ' and χ'' denote the real and imaginary components of the complex ferrofluid susceptibility $\chi = \chi' - i\chi''$. Here, τ refers to the relaxation time of the ferrofluid that is dependent on its material properties, and ω the angular frequency of the ac magnetic field. Thus, the particle magnetization

$$M(t) = H_0[\chi' \cos(\omega t) + \chi'' \sin(\omega t)]. \tag{7}$$

Substituting Eq. (7) into Eq. (2),

$$\Delta U = \omega\mu_0 H_0^2 \chi'' \int_0^{2\pi/\omega} \sin^2(\omega t) dt. \tag{8}$$

The power dissipation, P, due to magnetic heating is the product $f\Delta U$, i.e.,

$$P = f\Delta U = \mu_0 \pi \chi'' f H_0^2, \tag{9}$$

where $f = \omega/2\pi$.

B. Parametric investigation

We now investigate the influence of H_0, f, and R on MFH by assuming a lumped ferrofluid dosed tissue system. Its temperature variation[9]

$$dT/dt = P/(\rho c), \tag{10}$$

where ρ and c denote the ferrofluid density and heat capacity, respectively. Equation (10) is expressed in terms of a nondimensional temperature rise parameter

$$\begin{aligned}(dT/dt)^* &= (dT/dt)[R^2/(T_i\alpha)] = (\Delta T/\Delta t)[R^2/(T_i\alpha)] = \Delta T^*/\Delta t^* \\ &= [\mu_0\pi\chi_0 H_0^2/(\rho c T_i)](fR^2/\alpha)\{2\pi f\tau/[1 + (2\pi f\tau)^2]\} \\ &= t^*/(JF_0),\end{aligned} \tag{11}$$

where T_i denotes the initial temperature, α the thermal diffusivity of the tumor, and the * stands for nondimensional parameter. The Joule number J represents the ratio of the heating energy to the magnetic field energy, t^* is a normalized time, and F_0 the Fourier number defined as

$$F_0 = \alpha/(fR^2), \quad J = (\rho c T_i)/(\pi\mu_0\chi_0 H_0^2), \text{ and}$$

$$t^* = (2\pi f\tau)/[1 + (2\pi f\tau)^2]. \tag{12}$$

Equation (11) shows that the rate of change in ferrofluid temperature depends inversely on J. Hence, if the material and the particle size are specified and the frequency is held constant, $(dT/dt)^*$ varies quadratically with H_0. Next, we examine the behavior of t^*/F_0 for a representative MNP radius $R = 5$ nm, $\alpha = 0.132$ mm^2/s, determined from the material properties in Table I,[19] and an MNP volume fraction $\varphi = 2 \times 10^{-4}$. The initial tumor temperature T_i is assumed to be 37 °C. Figure 1 shows that t^*/F_0, thus dT/dt, varies qua-

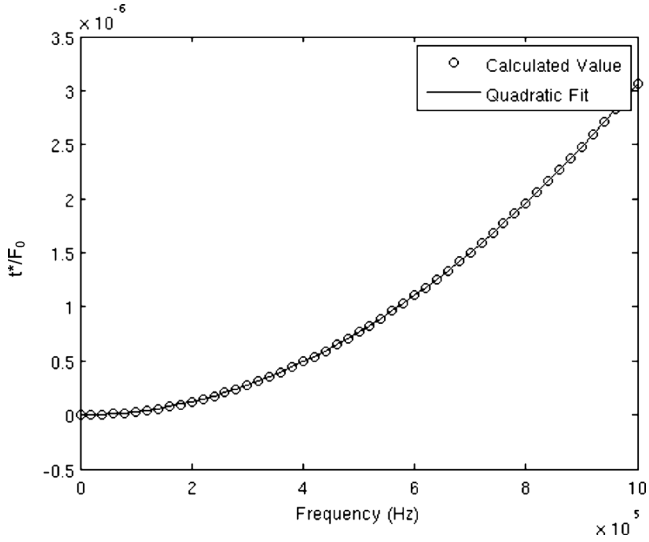

FIG. 1. Dependence of $(t^*/F_0)=J(dT/dt)^*$ on the frequency of the magnetic field for a constant J. The MNP radius $R=5$ nm, $\alpha=0.132$ mm^2/s with tissue properties as described in Table I.

dratically with the frequency when the field strength, i.e., J, is held constant. Therefore, MFH treatment is more effective at higher magnetic field strengths and frequencies with the limitation that high frequencies and strong magnetic fields can cause significant adverse affects on the human body above a maximum threshold.

C. Heating profiles of different ferrofluids

The power dissipation from a nanoparticle depends upon its magnetic susceptibility, which in turn is related to the ferrofluid relaxation time. Brownian relaxation occurs when the particle spins to align itself with the magnetic moment, while Néel relaxation occurs when the magnetic moment spins within the crystal structure of the nanoparticle,[9] where

$$\tau_B = 4\eta\pi(R+\delta)^3/kT, \tag{13}$$

$$\tau_N = \sqrt{\pi}/2\tau_0 \exp[4\kappa\pi R^3/(3kT)]/\sqrt{4\kappa\pi R^3/(3kT)}, \tag{14}$$

where η denotes the viscosity of the matrix fluid, δ the thickness of surfactant layer, τ_0 the Larmor time constant (=1 $\times 10^{-9}$ s), and κ the anisotropy constant. Both the Brownian and Néel relaxation times, denoted, respectively, by τ_B and τ_N, influence the total relaxation time τ of the particle, i.e.,

$$1/\tau = 1/\tau_B + 1/\tau_N. \tag{15}$$

We note from Eqs. (5), (13), and (14) that both M_{sat} and κ, which are material properties, contribute to the dissipated power. Therefore, we employ Eq. (10) to simulate the heating rates with different materials of varying particle sizes.

The maximum safe field strength that can be applied to humans is 15 kA/m.[3] For this reason, the simulated field strengths are specified to be 5, 10, and 15 kA/m. Frequencies of 150, 300, and 450 kHz are simulated to maintain the product $H \bullet f$ below the maximum threshold value of 4.85 $\times 10^{10}$ kA turns/(m s) allowable for humans.[24] Figures 2 and 3 show that higher frequencies and magnetic field strengths induce greater hyperthermia. However, taking patient safety into account, only values in the middle range of both the frequency and field strength are further investigated (i.e., 300 kHz and 10 kA/m, respectively).

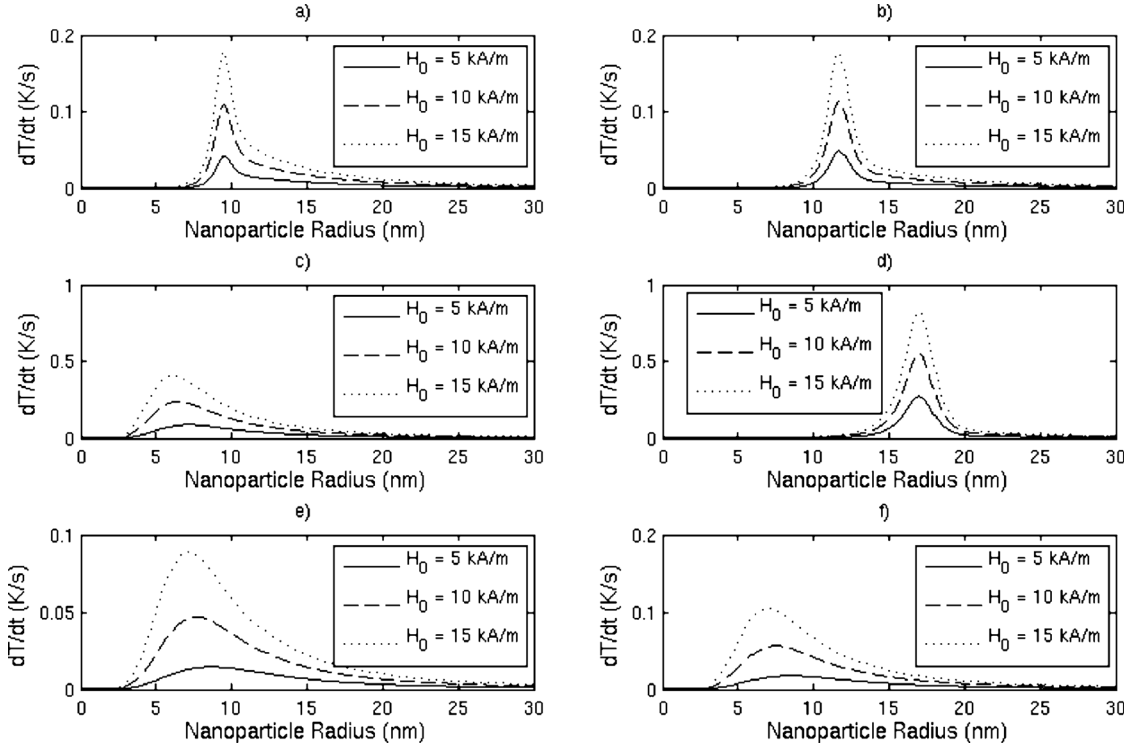

FIG. 2. Rate of change in temperature with respect to MNP radius for different H_0 and a constant 300 kHz magnetic field frequency for different MNP materials: (a) magnetite, (b) maghemite, (c) iron-platinum, (d) iron-cobalt, (e) barium-ferrite, (f) cobalt-ferrite.

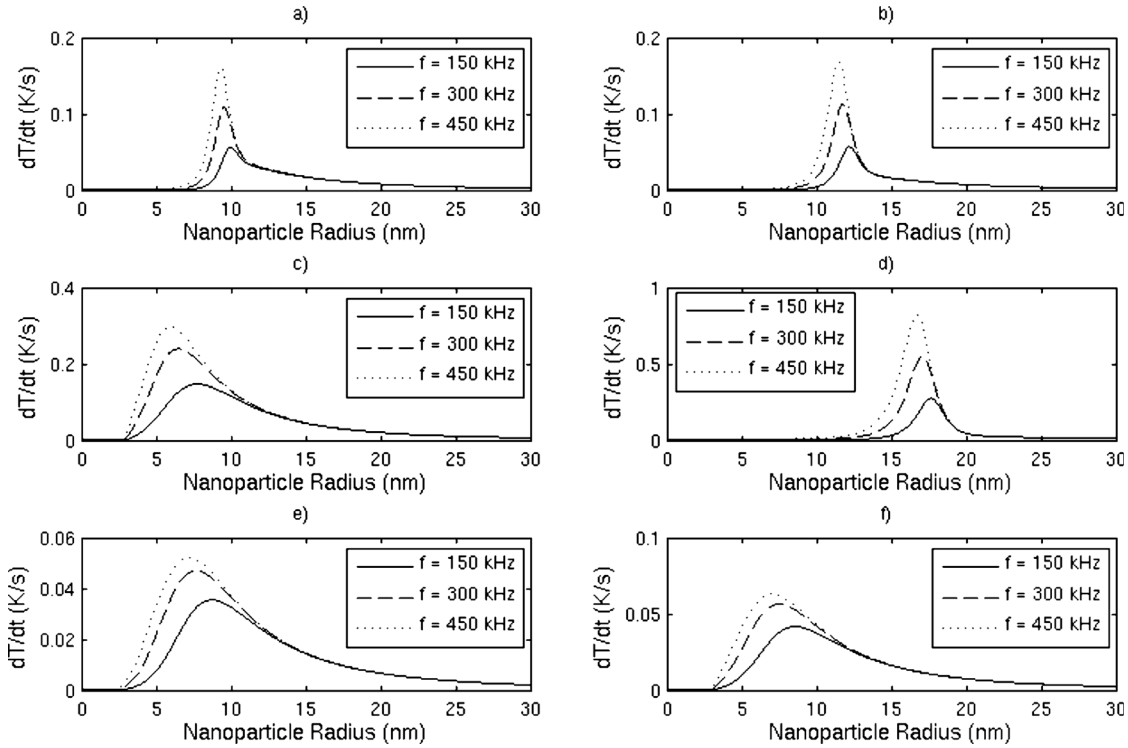

FIG. 3. Rate of change in temperature with respect to MNP radius for different magnetic field frequencies and constant $H_0=10$ kA/m for different MNP materials: (a) magnetite, (b) maghemite, (c) iron-platinum, (d) iron-cobalt, (e) barium-ferrite, (f) cobalt-ferrite.

D. Influence of nanoparticle radius

As seen from Eqs. (13) and (14), the nanoparticle size also plays an important role in determining the amount of heating that an MFH treatment can provide. Figures 2 and 3 show that each material has a critical radius for which dT/dt is maximum. This radius is recorded in the last column of Table II for the various materials. MNPs made of $BaFe_2O_4$ and $CoFe_2O_4$, are not suitable for MFH, since the maximum rate of temperature change for these materials is far too low. FeCo MNPs produce temperature changes that are too rapid to be safe for inducing controlled MFH. The remaining three MNPs are capable of producing reasonably rapid, yet controlled, temperature changes. Therefore, we examine the interaction of these latter three candidate materials with biological tissue.

We also consider the range of polydispersion that each type of material allows. Figures 2 and 3 show that some materials provide significant heating over a wider range of nanoparticle sizes than others do. For instance, large rates of temperature change occur over a wider range of radii for fcc FePt than for magnetite and maghemite. Defining $T'_{1/2}$ as half of the maximum value of dT/dt, the range of nanoparticle sizes that produce a temperature change rate greater than or equal to $T'_{1/2}$ are reported in Table III for $H_0=10$ kA/m and $f=300$ kHz.

For $BaFe_2O_4$, $CoFe_2O_4$, and fcc FePt, the induced temperature change rate is a reasonable fraction of the maximum temperature change over a range of over 5 nm. However, materials such as magnetite ($FeO\cdot Fe_2O_3$) and maghemite ($\gamma\cdot Fe_2O_3$) have a much smaller size range ($\approx$1.6 nm). This indicates that if magnetite and maghemite were to be used for MFH, the MNPs would have to be more monodisperse for adequate heating to occur while an MFH treatment using fcc FePt could allow for a larger polydisperse range of particle sizes.

III. ANALYSIS OF TISSUE HEATING IN MFH

A. Tumor model

Having identified the factors that influence the heating of different MNPs, we now examine tissue heating in an MFH

TABLE II. Properties of MNPs (Refs. 9 and 19).

Magnetic solid	M_{sat} (kA/m)	κ (kJ/m^3)	c (J/kg/K)	ρ (kg/m^3)	R (nm)
Magnetite	446	23	670	5180	9.5
fcc FePt	1140	206	327	15 200	6.4
Maghemite	414	4.7	746	4600	11.7
FeCo	1790	1.5	172	8140	17.0
$CoFe_2O_4$	425	180	700	4907	7.5
$BaFe_2O_4$	380	300	650	5280	7.6

TABLE III. Allowable range of polydispersion of nanoparticles.

Magnetic solid	$T'_{1/2}$ (K/s)	r_{min} (nm)	r_{max} (nm)
Magnetite	0.0547	8.8	10.4
fcc FePt	0.1198	4.5	10.2
Maghemite	0.0565	10.9	12.5
FeCo	0.2750	15.9	18.0
$CoFe_2O_4$	0.0235	4.8	12.9
$BaFe_2O_4$	0.0282	5.4	11.3

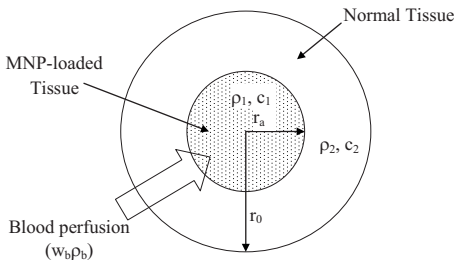

FIG. 4. Schematic diagram of a ferrofluid-loaded tumor. The shaded inner cross section represents tumor tissue loaded with MNPs, and the outer cross section the surrounding healthy tissue without MNPs.

application for the idealized geometry of a spherical tumor tissue shown in Fig. 4. The tumor is selectively loaded with MNPs while the healthy tissue surrounding it contains no nanoparticles. A perfusion term considers heat transfer to the blood as being proportional to the volumetric blood flow and the difference between the local tissue and the arterial temperatures.[25,26] The blood temperature is always 37 °C, a reasonable assumption since it travels rapidly enough to be relatively unaffected by any heating.[27] The blood perfusion is homogeneous throughout the healthy and affected tissue, since blood capillaries are typically homogeneously distributed in the tissue bed.[28] The MNP-loaded tissue experience a volumetric heating under an alternating magnetic field, while the perfusing blood abstracts heat from the tissue as long as the tissue temperature is above a threshold (the basal body temperature). In order to determine the heating of biological tissue, we use a mathematical model based on the Pennes bioheat transfer equation,[19] i.e.,

$$\rho_1 c_1(\partial T_1/\partial t) = (\lambda_1/r^2)\,\partial/\partial r(r^2\,\partial T_1/\partial r) + w_{b1}\rho_b c_b(T_b - T_1) + q_{met} + P, \quad 0 \le r \le r_a, \tag{16}$$

and

$$\rho_2 c_2(\partial T_2/\partial t) = (\lambda_2/r^2)\,\partial/\partial r(r^2\,\partial T_2/\partial r) + w_{b2}\rho_b c_b(T_b - T_2) + q_{met}, \quad r_a < r \le r_o, \tag{17}$$

where r denotes the radial distance, λ the thermal conductivity, w_b the blood perfusion, q_{met} metabolic heat generation (taken as 540 W), and the subscripts 1, 2, and b stand for tumor tissue loaded with MNPs, tumor tissue without MNPs, and blood, respectively. The values for ρ_2 and c_2 are provided in Table I while $\rho_1=(1-\varphi)\rho_2+\varphi\rho$ and $c_1=(1-\varphi)c_2+\varphi c$, where ρ and c, respectively, denote the density and heat capacity of the nanoparticle being used. As illustrated in Fig. 4, r_a denotes the radius of the region of tumor tissue loaded with MNPs, and r_o the domain of the model. The inner boundary condition for Eq. (16) is imposed through a zero temperature gradient due to spherical symmetry at $r=0$. A convection heat balance boundary condition is imposed at the interface of the edge of the healthy tissue at $r=r_o$. An initial condition that assumes a uniform temperature distribution equal to the arterial blood temperature (37 °C), precedes the application of the alternating magnetic field. A finite difference scheme is used to solve Eqs. (16) and (17). The solution methodology is described in Appendix. The simulation is conducted with a homogeneous grid of 500 cells, which provides grid independent results.

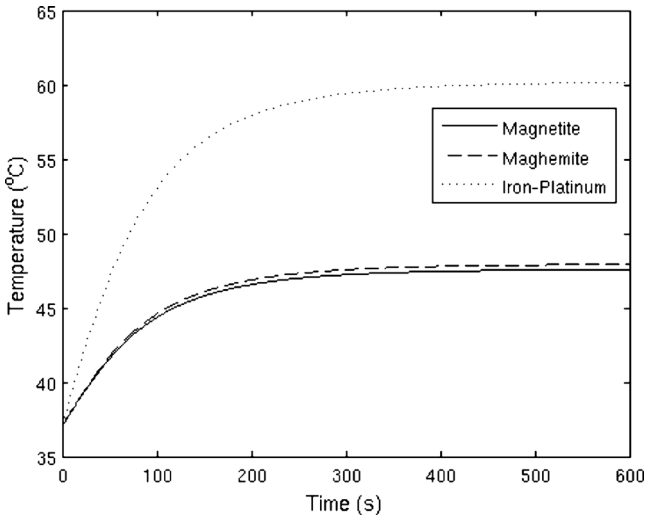

FIG. 5. Evolution of the temperature at the center of a 10 mm tumor over time for continuous hyperthermia with $H_0=10$ kA/m and a frequency $f=300$ kHz. The MNP radius corresponds to the critical radius R reported in Table II.

B. Influence of nanoparticles material on tumor heating

Simulations are conducted with identical loadings ($\varphi=0.02\%$) of the three different nanoparticle materials. The material properties for the tissue are described in Table I and those for the MNPs required to determine P are taken from several sources in the literature and listed in Table II.[9,19,29] We assume that the MNPs are monodispersed and have a size equal to the critical radius at which dT/dt is maximum (as discussed in Sec. II D; the radius R is reported in Table II), that the imposed magnetic field has a strength of $H=10$ kA/m and a frequency of $f=300$ kHz, the ferrofluid has a viscosity of 6.53×10^{-4} Pa s at 37 °C, and the surfactant thickness is 1 nm.[17] Each simulation is performed until the tissue temperature reaches a steady state. For the sake of illustration, $r_a=1$ cm while $r_o=10$ cm. A steady blood infusion rate of 6.4 s^{-1} is assumed for all the simulations.[9]

1. Magnetite

The material constants for magnetite[9] in Table II are used to obtain the results shown in Figs. 5 and 6. The temporal evolution of the tumor center temperature presented in Fig. 5 shows a rapid initial increase which soon stabilizes to a nearly constant value. The maximum temperature reached by magnetite particles is slightly greater than 47 °C at the tumor center, which is well above the minimum required temperature required for MFH. Figure 6 shows that the temperature at $r=1$ cm, i.e., at the tumor-healthy tissue interface, reaches a maximum value of ≈40 °C. This implies that while almost all of the tumor tissue can be subjected to hyperthermia, no healthy tissue will be damaged, since the temperatures lie below 41 °C for $r>1$ cm.

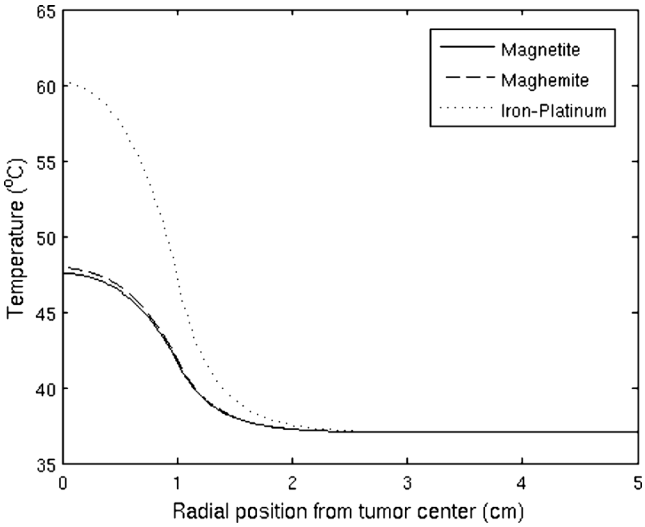

FIG. 6. Radial temperature distribution after 600 s of continuous heating for a 10 mm tumor. Other parameters are as described in Fig. 5.

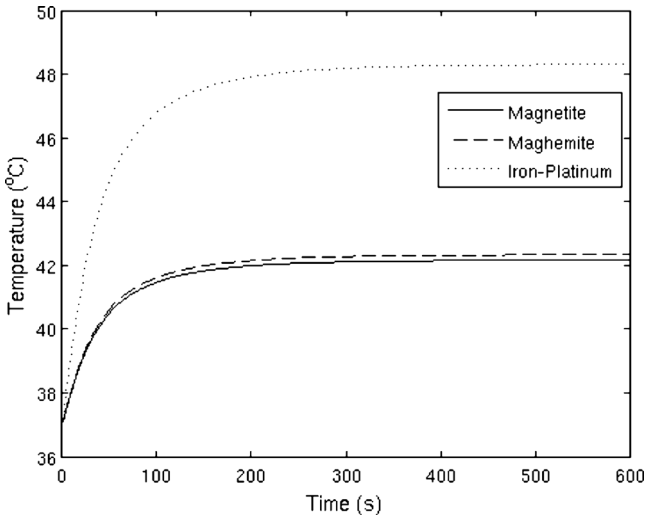

FIG. 7. Time evolution of the temperature at the center of a 5 mm tumor for continuous hyperthermia using $H_0=10$ kA/m and a frequency $f=300$ kHz. The MNP radius corresponds to the critical radius R reported in Table II.

2. Iron-platinum

The material properties for fcc FePt are obtained from the literature.[19] Figure 5 shows that the temperature increase during MFH with fcc FePt is significantly more rapid than with magnetite. However, the eventual steady state temperatures are almost equivalent even though FePt produces slightly higher heating. At the tumor center, the temperature rises to above 60 °C while it is ≈47 °C at the tumor-healthy interface. The temperature falls below 41 °C a short distance of 1.28 cm removed from the interface into the healthy tissue. This has the unintended consequence of harming a small section of the surrounding tissue along with the tumor cells.

3. Maghemite

Figure 5 shows that maghemite MNPs induce slightly slower heating of the tissue than with magnetite. At the tumor center, the temperature increases to just above 47 °C. The temperature at the tumor-healthy interface is ≈41 °C. This is promising since all of the tumor cells reach a high enough temperature to induce hyperthermia while the surrounding healthy tissue is preserved.

C. Effects of tumor size

While these results, especially those for magnetite and fcc FePt, are in good agreement with some literature,[19] other investigations indicate that the temperature increases for these cases might be much smaller.[30] In order to reconcile these differences, we simulate MFH for a smaller tumor with $r_a=5$ mm but keeping the other conditions the same. Figures 7 and 8 show the corresponding temporal growth of the tissue center temperature, and the steady state temperature distribution, respectively. Since the tumor radius is now half its previous value, the number of nanoparticles it contains decreases by an eighth. This produces significantly lower heating, which is evident by comparing Figs. 5 and 7 or Figs. 6 and 8. In Fig. 7, the tumor center temperature increases at a slower rate for all the three nanoparticles.

However, a quasisteady state is reached sooner for the 5 mm radius tumor than its 10 mm counterpart. Comparison of Figs. 7 and 8 indicates that the temperatures both at tumor center and tumor-healthy tissue interface are lower for the 5 mm radius tumor.

The simulations indicate that tumor size has a significant effect on the ability of MNPs to heat cancerous tissue. While iron-platinum is still capable of producing hyperthermia for the smaller radius tumor, neither magnetite nor maghemite produce enough heating for the tumor-healthy interface to reach 41 °C. The temperature at the tumor-healthy interface is presented in Fig. 9 for a range of tumor radii. Iron-platinum produces hyperthermia at tumor sizes of 5 mm or larger but magnetite and maghemite require tumor sizes of 11 mm and 10 mm, respectively, in order to effectively expose all of the cancer cells to MFH. To treat tumor sizes smaller than 5 mm would require an increase in the ferrofluid volume fraction, since increasing the magnetic field strength

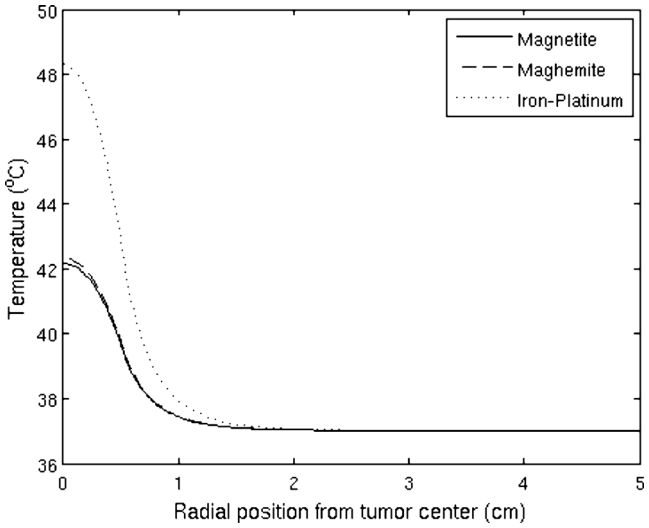

FIG. 8. Radial temperature distribution after 600 s of continuous heating for a 5 mm tumor. Other parameters are as described in Fig. 5.

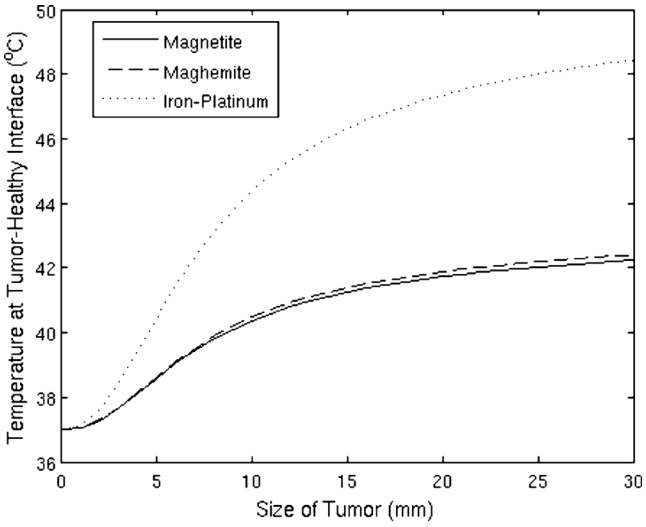

FIG. 9. Temperature at the interface of the tumor and healthy tissue after 600 s of continuous hyperthermia as a function of the tumor radius.

or frequency might lead to unsafe conditions for the patient. Although the number of nanoparticles varies as r^3 for specified φ, the effect of changing radius on the temperature at the tumor-healthy interface does not scale similarly above $r=3$ mm. As both the interface and average tumor temperatures increase, the heat loss from the tumor due to blood perfusion also increases. Thus, as the tumor radius becomes larger than 3 mm, the increase in the interface temperature is more gradual with increasing tumor size, as shown in Fig. 9.

In order to distinguish whether the enhanced heating is related to an increase in tumor size or occurs simply due to a larger number of nanoparticles, we simulated MFH for tumors with different radii and magnetite nanoparticle volume fractions. These results are shown through the contour plots in Fig. 10 for tumor radii in the 0–30 mm range and particle volume fractions of 0%–0.04%. The vertical dotted line in Fig. 10 represents the condition for magnetite particles described in Fig. 9. The interface temperature becomes less

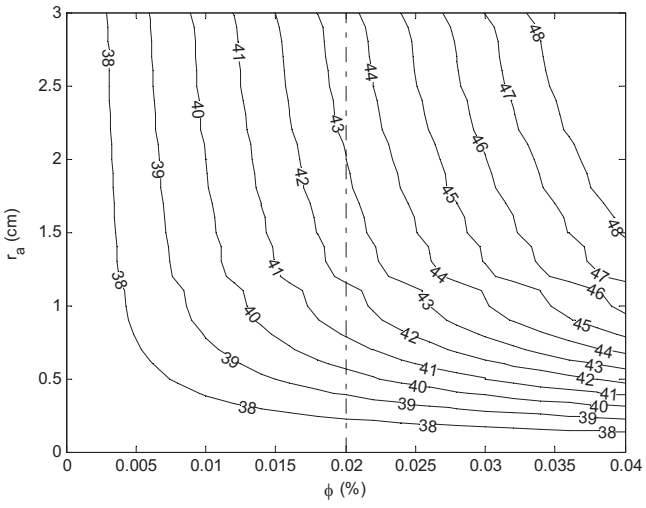

FIG. 10. Contour plots of the temperatures at the tumor-healthy tissue interface for varying tumor sizes and the nanoparticle volume fractions φ. The vertical dotted line corresponds to the conditions reported in the magnetite-loaded tissue surface temperature plot of Fig. 9.

sensitive to larger tumor radii, which is consistent with Fig. 9, although the temperature always increases with increasing radius.

This loss of sensitivity of the interfacial temperature to tumor size is attributed to the increased perfusion heat loss for larger tumors, which is also more significant for smaller nanoparticle loading. For example, when the particle loading is lower than 0.005%, the tumor-healthy tissue interface temperature is virtually insensitive to increasing tumor radius when $r_a > 0.8$ cm. To raise this temperature for larger tumors, φ must be increased. However, increasing φ for smaller tumors does not follow a similar trend. The implication is that it is not possible to induce hyperthermia in tumors that are exceedingly small. Figure 10 is useful as a quick guide to select suitable particle loadings that will heat a tumor of a particular size optimally. Combinations of φ and r_a selected from Fig. 10 provide optimal MFH conditions, i.e., when only the tumor is treated and no healthy tissue is damaged.

IV. CONCLUSIONS

We investigated the thermal response of six ferrofluid materials, magnetite, maghemite, fcc iron-platinum, iron-cobalt, barium-ferrite, and cobalt-ferrite, on a tissue undergoing MFH. Iron-cobalt MNPs induce temperature changes that are too large, whereas barium-ferrite and cobalt-ferrite MNPs do not provide enough heat to treat a tumor. The heating from MNPs dissipates within a relatively small distance from the center of a perfused tumor, which can be used advantageously to preserve the surrounding healthy tissue. Our simulations show that magnetite, fcc iron-platinum, and maghemite MNPs are well suited for MFH, making it possible to heat tumors above 41 °C while keeping the surrounding healthy tissue temperatures below this value. The temperature at the tumor-healthy tissue interface falls below the threshold value for small tumor radii, which require larger MNP volume fractions for successful MFH. The tumor surface temperature increases as r_a^3 for small tumors but this rate of increase declines at larger radii due to the more pronounced heat loss through blood perfusion.

APPENDIX

Since metabolic heat generation q_{met} is much smaller than the other terms in the governing equations (roughly 540 W over the entire human body),[19] we neglect its effects. The boundary conditions to the partial differential equations are zero gradient at the center and a convection heat transfer at $r=r_o$, while the initial condition is a uniform temperature distribution equal to the arterial blood temperature (37 °C).

In order to solve Eqs. (16) and (17) for T_1 and T_2, we consider

$$\rho_1 c_1(\partial T_1/\partial t) = (\lambda_1/r^2)\,\partial/\partial r(r^2\,\partial T_1/\partial r) + w_{b1}\rho_b c_b(T_b - T_1) + P, \quad 0 \le r \le r_a, \tag{A1}$$

$$\rho_2 c_2(\partial T_2/\partial t) = (\lambda_2/r^2)\,\partial/\partial r(r^2\,\partial T_2/\partial r) + w_{b2}\rho_b c_b(T_b - T_2), \quad r_a < r \le r_o, \tag{A2}$$

$$\lambda_2(\partial T_2/\partial r)|_{r=r_0} + hT(r_0,t) = hT_\infty. \quad \text{(A3)}$$

A central differencing scheme is used to discretize Eqs. (A1) and (A2) at every node, including the boundary nodes. The boundary condition of zero temperature gradient at $r=0$ is imposed by using a fictitious node and prescribing $T^n_{-1}=T^n_1$ in the discretized governing equation at $r=0$. In order to avoid the singularity at $r=0$, Eq. (A1) is replaced at $r=0$ with

$$(\rho_1 c_1/\lambda_1)(\partial T_1/\partial t) = 3[\partial/\partial r(\partial T_1/\partial r)] + w_{b1}c_b/\lambda_1[(T_b - T_1) + P\lambda_1/(w_{b1}c_b)] \quad \text{for } r=0 \quad \text{(A4)}$$

The discretized form of Eq. (A4) is

$$T_0^{n+1} = \{1 - 6[\lambda_1/(\rho_1 c_1)](\Delta t/\Delta r^2)\}T_0^n + 6[\lambda_1/(\rho_1 c_1)] \times (\Delta t/\Delta r^2) + [\Delta t/(\rho_1 c_1)]w_{b1}c_b[(T_b - T_0^n) + P\lambda_1/(w_{b1}c_1)]. \quad \text{(A5)}$$

Similarly, the far end (i.e., $r=r_o$) convective boundary condition [Eq. (A3)] is specified using a fictitious cell after the farthest node.

The discretized equation for any internal node (i.e., for $0<r<r_0$) is

$$T_i^{n+1} = [\lambda_1/(\rho_1 c_1)](\Delta t/\Delta r^2)(1 - \Delta r/r)T_{i-1}^n + \{1 - 2[\lambda_1/(\rho_1 c_1)](\Delta t/\Delta r^2)\}T_i^n + [\lambda_1/(\rho_1 c_1)](\Delta t/\Delta r^2) \times (1 + \Delta r/r)T_{i+1}^n + [\Delta t/(\rho_1 c_1)](w_{b1}c_b)[(T_b - T_i^n) + (P\lambda_1)/(w_{b1}c_1)]. \quad \text{(A6)}$$

For $r>r_a$, Eq. (A6) is rewritten by replacing all terms with a subscript 1 with the corresponding terms with subscript 2, and setting $P=0$.

[1] E. S. Day, J. G. Morton, and J. L. West, ASME J. Biomech. Eng. **131**, 074001 (2009).
[2] P. Tartaj, M. D. Morales, S. Veintemillas-Verdaguer, T. Gonzalez-Carreno, and C. J. Serna, J. Phys. D: Appl. Phys. **36**, R182 (2003).
[3] Q. A. Pankhurst, J. Connolly, S. K. Jones, and J. Dobson, J. Phys. D: Appl. Phys. **36**, R167 (2003).
[4] L. E. Gerlowski and R. K. Jain, Microvasc. Res. **31**, 288 (1986).
[5] A. H. Habib, C. L. Ondeck, P. Chaudhary, M. R. Bockstaller, and M. E. McHenry, J. Appl. Phys. **103**, 07A307 (2008).
[6] R. Hergt, R. Hiergeist, I. Hilger, W. A. Kaiser, Y. Lapatnikov, S. Margel, and U. Richter, J. Magn. Magn. Mater. **270**, 345 (2004).
[7] R. Hiergeist, W. Andra, N. Buske, R. Hergt, I. Hilger, U. Richter, and W. Kaiser, J. Magn. Magn. Mater. **201**, 420 (1999).
[8] Y. Rabin, Int. J. Hyperthermia **18**, 194 (2002).
[9] R. E. Rosensweig, J. Magn. Magn. Mater. **252**, 370 (2002).
[10] J. H. Gao, H. W. Gu, and B. Xu, Acc. Chem. Res. **42**, 1097 (2009).
[11] M. Suto, H. Kosukegawa, K. Maruta, M. Ohta, K. Tohji, and B. Jeyadevan, J. Magn. Magn. Mater. **321**, 3483 (2009).
[12] R. K. Gilchrist, R. Medal, W. D. Shorey, R. C. Hanselman, J. C. Parrott, and C. B. Taylor, Ann. Surg. **146**, 596 (1957).
[13] P. Moroz, S. K. Jones, and B. N. Gray, Int. J. Hyperthermia **18**, 267 (2002).
[14] L. L. Lao and R. V. Ramanujan, J. Mater. Sci.: Mater. Med. **15**, 1061 (2004).
[15] W. Andrä, C. G. d'Ambly, R. Hergt, I. Hilger, and W. A. Kaiser, J. Magn. Magn. Mater. **194**, 197 (1999).
[16] J. W. Durkee, P. P. Antich, and C. E. Lee, Phys. Med. Biol. **35**, 847 (1990).
[17] H. G. Bagaria and D. T. Johnson, Int. J. Hyperthermia **21**, 57 (2005).
[18] C. T. Lin and K. C. Liu, Int. Commun. Heat Mass Transfer **36**, 241 (2009).
[19] S. Maenosono and S. Saita, IEEE Trans. Magn. **42**, 1638 (2006).
[20] A. Skumiel, Int. J. Thermophys. **28**, 1461 (2007).
[21] D. L. Huber, Small **1**, 482 (2005).
[22] K. Okawa, J. Appl. Phys. **99**, 08H102 (2006).
[23] R. Ganguly and I. K. Puri, WIREs Nanomedicine & Nanobiotechnology **2**, 382 (2010).
[24] W. Atkinson, IEEE Trans. Biomed. Eng. **BME-31**, 70 (1984).
[25] H. Arkin, L. X. Xu, and K. R. Holmes, IEEE Trans. Biomed. Eng. **41**, 97 (1994).
[26] E. H. Wissler, J. Appl. Physiol. **85**, 35 (1998).
[27] P. Yuan, Int. J. Heat Mass Transfer **52**, 1734 (2009).
[28] F. Kreith, *The CRC Handbook of Thermal Engineering* (CRC, Boca Raton, FL, 2000).
[29] A. Candeo and F. Dughiero, IEEE Trans. Magn. **45**, 1658 (2009).
[30] L. Zhang, J. J. Abbott, L. X. Dong, B. E. Kratochvil, D. Bell, and B. J. Nelson, Appl. Phys. Lett. **94**, 064107 (2009).